HHS Public Access

Author manuscript

ACS Catal. Author manuscript; available in PMC 2018 June 19.

Published in final edited form as:

ACS Catal. 2017 June 2; 7(6): 3916–3923. doi:10.1021/acscatal.7b01286.

Mechanism of chloride inhibition of bilirubin oxidases and its dependence on potential and pH

Anne de Poulpiquet[a], **Christian H. Kjaergaard**[b], **Jad Rouhana**[c,d], **Ievgen Mazurenko**[a], **Pascale Infossi**[a], **Sébastien Gounel**[c,d], **Roger Gadiou**[e], **Marie Thérèse Giudici-Orticoni**[a], **Edward I. Solomon**[*,b], **Nicolas Mano**[*,c,d], and **Elisabeth Lojou**[*,a]

[a]Aix Marseille Univ, CNRS, BIP, 31 chemin Aiguier, 13402 Marseille, France

[b]Department of Chemistry, Stanford University, Stanford, California 94305, United States

[c]CNRS, CRPP, UPR 8641, 33600 Pessac, France

[d]Univ. Bordeaux, CRPP, UPR 8641, 33600 Pessac, France

[e]Institut des Sciences de Matériaux de Mulhouse, CNRS, 15 rue Starcky, 68057 Mulhouse, France

Abstract

Bilirubin oxidases (BODs) belong to the multi-copper oxidase (MCO) family and efficiently reduce O_2 at neutral pH and in physiological conditions where chloride concentrations are over 100 mM. BODs were consequently considered to be Cl^- resistant contrary to laccases. However, there has not been a detailed study on the related effect of chloride and pH on the redox state of immobilized BODs. Here, we investigate by electrochemistry the catalytic mechanism of O_2 reduction by the thermostable *Bacillus pumilus* BOD immobilized on carbon nanofibers in the presence of NaCl. The addition of chloride results in the formation of a redox state of the enzyme, previously observed for different BODs and laccases, which is only active after a reductive step. This behavior has not been previously investigated. We show for the first time that the kinetics of formation of this state is strongly dependent on pH, temperature, Cl^- concentration and on the applied redox potential. UV-visible spectroscopy allows us to correlate the inhibition process by chloride with the formation of the alternative resting form of the enzyme. We demonstrate that O_2 is not required for its formation and show that the application of an oxidative potential is sufficient. In addition, our results suggest that the reactivation may proceed thought the T3 β.

Introduction

Bilirubin oxidases (BODs) belong to the multicopper oxidase family (MCOs) and couple the oxidation of bilirubin to the reduction of oxygen to water through four copper centers, one type 1 Cu (T1) and a trinuclear center (TNC) composed of one type 2 Cu and a coupled

*Corresponding Author: lojou@imm.cnrs.fr, mano@crpp-bordeaux.cnrs.fr, solomone@stanford.edu.

Supporting Information. Electrochemical characterization of O_2 reduction in various conditions is given in Figures SI1-SI8. This material is available free of charges via Internet at http://pubs.acs.org.

The authors declare no competing financial interests.

binuclear type 3 Cu center. Substrate oxidation and O_2 reduction take place at the T1 and TNC respectively.[1–3] The overall accepted mechanism for O_2 reduction involves the binding of O_2 to the reduced TNC, a two electron reduction step to form a peroxy intermediate (PI), cleavage of the O-O bound which yields the native intermediate state (NI). Four electron reduction of NI regenerates the fully reduced enzyme (Scheme 1).[2,4,5,6,7] Different resting forms of MCOs have been identified by spectroscopies and electrochemistry. One of these corresponds to a fully oxidized resting form, derived from the decay of NI that involves the loss of a μ_3-O bridge.[2,6,7] Another resting state, called alternative resting form (AR), was identified in some MCOs, such as BOD CotA from *Bacillus subtilis*.[8] These two resting forms were shown to exist in BODs from *Magnaporthe oryzae* and *Myrothecium verrucaria*.[9,10] In AR, the spectroscopic signatures of the TNC were unusual, especially lacking the 330 nm charge transfer transition originating from a bridging hydroxide ligand. It was demonstrated that the TNC is partially reduced (2x Cu(I) and 1x Cu(II)) while the T1 is oxidized.[10] The oxidized Cu in the TNC was suggested to be one of the T3 Cu, denoted T3 β, which would have a lower potential than the T1 Cu. In this AR form, T2 and T3 α of the TNC would be reduced.[11]

Electrochemistry can provide essential information on the mechanisms and states of the enzymes involved during heterogeneous catalysis, provided that an electrical connection between the biological molecules and the electrode is achieved. Direct electron transfer (DET) between BOD - or its parent enzyme laccase – and electrochemical interfaces was obtained *via* appropriate modifications of electrode surfaces.[12,13] The most targeted configuration involved electrical connection of the T1, characterized in the absence of O_2 by a non-catalytic redox signal at the expected potential of the T1 Cu. In the presence of O_2, a single catalytic wave for O_2 reduction is observed, consistent with the electrode replacing the electron-donating substrate. In rare cases, a proper orientation on the electrode allowed bypass of the natural pathway to provide electrons directly to the TNC. Different situations were observed, *i.e.* two successive waves attributed to the successive O_2 reduction by DET to the T1 then to the TNC,[14] or one unique catalytic wave at a potential attributed to DET to the TNC[15]. However, in most cases where DET to the T1 was not allowed, the TNC was also not connected. As a consequence catalysis *via* only the TNC sparing electron transfer from/to the T1 was not observed.[16,17,18] Favoring one or the other catalytic process seems to be essentially dependent on the chemical modification of the electrode which yields a specific orientation of the enzyme.

Due to their ability to reduce O_2 under physiological conditions (pH 7, 140 mM NaCl, 37°C), BODs are the cathodic enzymes of choice in enzymatic fuel cells for implantation applications.[19,20] Since they are highly active at neutral pH, they are often preferred to laccases that are only active at acidic pH. BOD activity in the presence of huge chloride concentrations suggested that they were insensitive to chloride.[21–23] However, few studies described the associated resistance mechanisms. An early publication demonstrated that halides do actually inhibit BOD from *Trachyderma tsunodae* K-25. It was suggested that halides bind at the TNC center, preventing the intramolecular electron transfer.[24] In the presence of halides, UV-visible spectra of BODs showed an increase in the intensity of the band at 600 nm arising from a charge transfer transition on the T1 and a decrease of the shoulder at 330 nm. These spectral changes resemble the signature of the AR state. It was

hypothesized that changes in the redox potential of the TNC due to the halide binding may induce a disproportion of electrons between T1 and TNC. The discrepancies between these conclusions may arise from the pH at which the inhibition studies were carried out. As support of this assessment, a nice study from Dagys *et al.*[25] recently reported the influence of fluoride addition as a function of pH on the catalytic O_2 reduction by a fungal laccase. A different catalytic inhibition process was observed depending on the connection of the enzyme to the electrode surface through the T1 or the TNC.

These fundamental data, in addition to the applications interest in BODs for implantable biofuel cells, require in-depth studies of the inter-relation between catalytic activity, enzyme states, halide inhibition and pH. We recently identified a new BOD from *B. pumilus*[26] and successfully used it for the design of an O_2 cathode[27, 28] and for the elaboration of a new generation of enzymatic H_2/ O_2 fuel cells.[29] By combining electrochemistry and spectroscopy, we investigate in the present study the inhibition of O_2 reduction by chlorides in *B. pumilus* BOD immobilized on carbon nanofibers (CNF). We highlight the chloride influence on the interconversion between the alternative resting and resting oxidized forms, and the involvement of these states in the catalytic cycle including the possibility of DET to the TNC.

Results and discussion

B. pumilus BOD was adsorbed on a graphite electrode modified with CNFs as reported earlier.[29] Relevant information can be extracted from the catalytic voltammograms of the immobilized enzyme, especially because this technique ensures control of the redox potential. It allowed, in particular, investigation of the mechanism of O_2 reduction by MCOs on electrodes.[7,30] Experiments were first conducted at pH 4 because we previously demonstrated that this was the optimum pH for direct O_2 reduction by *B. pumilus* BOD.[29] Before NaCl addition, the onset for O_2 reduction is observed at E_1 = +0.56 V vs Ag/AgCl (Fig 1, blue curve). The onset potential follows a constant decrease of 0.05 V per pH unit (Fig. SI1). Since a potential difference of ca. 100 mV can be observed for the onset potential with *M. verrucaria* BOD against *B. pumilus* BOD[17], and *M. verrucaria* BOD T1 Cu potential has been determined to be 460 mV at pH 7[32], we conclude that catalysis proceeds via T1 Cu in the absence of NaCl.

A sigmoidal wave typical of the catalytic reduction of O_2 is observed as cyclic voltammetry proceeds.[29, 31] After addition of NaCl to the electrolyte, the voltammogram is characterized by a hysteresis (Fig 1, red curve). On the forward scan, the onset for O_2 reduction shifts 360 mV more negative and is observed at E2 = +0.2 V vs Ag/AgCl. The reverse scan is less affected by NaCl, showing that O_2 reduction is far more efficient after the enzyme has been exposed to reducing potentials. This peculiar CV shape reflects an inactivation/reactivation process of BOD for O_2 reduction. We recorded the same effect with the thermostable *B. subtilis* BOD which shares 67% identity with *B. pumilus* BOD (data not shown). A role of a specific interaction between the CNF network and BOD on the inactivation/reactivation process can be ruled out since a similar behavior is obtained when *B. pumilus* BOD is directly adsorbed on a bare pyrolytic graphite electrode (Fig SI2). Interestingly, this behavior is very different from that reported by Dagys *et al.* for the influence of F^- on O_2 reduction

by a high-potential laccase.[25] In this particular case, the CVs exhibited a 100 mV potential shift of the onset potential for the first fluoride addition, and then a progressive decrease in the catalytic current upon increasing the concentration of F^-. No reactivation occurred at low potential. We observed a similar behavior with *B. pumilus* BOD in the presence of F^-, i.e. a small shift in the onset potential less than 100 mV, and progressive decrease in the catalytic current with no reactivation process at low potential. Those results highlight that two different mechanisms are involved depending on the type of halide (Fig. SI3).

Even after NaCl removal from the electrolyte, reductive activation at a potential below E2 is required to reactivate the NaCl-inhibited BOD. The onset for O_2 reduction occurs at E1 only along the second consecutive CV scan (Fig SI4). In the case of F^- this reductive activating step was not necessary in agreement with the preceding observations (data not shown). The peculiar CV shape in the presence of chloride with a reactivating process at low potential may be attributed to the coexistence of the two resting forms of the enzyme, i.e. fully oxidized RO and partially oxidized AR, as suggested in *M. oryzae* BOD.[10] To identify the redox states of the *B. pumilus* BOD, UV-Visible spectra were recorded following a protocol described earlier[10] in the absence or presence of NaCl. The typical shoulder at 330 nm of the as isolated BOD at pH=4 disappears upon NaCl addition (Fig 2A).

By analogy with our previous work[10,11], we conclude that the as isolated BOD is in the RO form, and is converted to the AR form upon Cl^- addition. At pH 7 (Fig 2B) however, in the time scale of the experiment, the BOD remains in its oxidized resting state even after addition of Cl^-. This result is the first evidence that the interconversion between the two resting forms induced by NaCl addition is pH dependent.

The coexistence of these two distinct resting forms of *B. pumilus* BOD is also evidenced by the CV shape in Fig 1. The first form, which is active for O_2 reduction at high potentials, derives from the RO form. O_2 reduction takes place at the redox potential E1 of the T1 Cu. The second form, which appears upon NaCl addition and requires an activation step at low potentials for O_2 reduction, corresponds to the partially reduced AR form in which T2 and T3α of the TNC are reduced and T3β is oxidized.[11] To assess the catalytic pathway in the two resting forms, we recorded under N2 the non-catalytic signals of the metallic centers, for the as isolated form, the AR form obtained after NaCl addition under O_2, and the reactivated form as described in Fig. SI4. Fig 3A shows the occurrence of a redox peak at 550 mV vs Ag/AgCl in the as isolated form, which disappears upon NaCl addition, and is partially recovered after enzyme reactivation. These observations reinforce the idea that in the usual catalytic cycle, direct connection with the electrode is established with the Cu T1. Two different explanations can account for the disappearance of the electrochemical signal upon Cl^- addition. It could be hypothesized that the reactivation of the AR form occurs *via* the Cu T1 presenting a lower potential induced by Cl^- binding. However, we were not able to detect such a shift in the Cu T1 redox potential. This first hypothesis cannot be totally ruled out since surface redox entities on the carbon nanofibers themselves might hide this redox process. The second hypothesis is that the Cu T1 is no longer connected to the electrode. In this latter case, in full agreement with our previous work, the reactivation of the AR form would proceed through direct electron transfer to the T3β Cu. Indeed, we recently demonstrated that the full reduction of the AR form of a laccase cannot occur via the T1, but

via the T3β.[11] A DET process through the TNC supposes that it is sufficiently close to the interface to exchange electrons with this latter. Such a direct connection is not unexpected as it was already detected in recent works.[15, 25] Moreover, simple structural considerations indicate that the T3β is located less than 15 Å from the *B. pumilus* BOD surface, making it accessible to electronic tunnelling from the electrode as described by Page *et al.*[33] (Figure 3B).

The conditions required for the conversion of the two resting forms were then examined by following the evolution of the CVs for a given incubation time at different NaCl concentrations (Fig 4A) and for a given NaCl concentration after different incubation times (Fig SI5).

Fig 4A shows a progressive change in the CV profile as NaCl concentration increases for 15 min incubation time. Between the CV profile in the absence of NaCl (blue curve) and the CV profile obtained for NaCl ≥ 20 mM (red curve), an intermediary shape is observed where O_2 reduction occurs at E1, but with a slow rate until E_2 is reached (green curve). The inactivation process is kinetically controlled. As shown in Fig. SI5, the state obtained in Fig 4A for 5 mM NaCl concentration is only an intermediate case. For longer time of incubation in the same electrolyte, the stationary state is characterized by O_2 reduction at E2 indicating the formation of the AR state. This is further supported by chronoamperometry experiments at +0.3 V (a potential between E1 and E2 over the pH range) which show that the inhibition kinetics increases with increasing NaCl concentrations (Fig 4B). The inhibition rates are calculated to be 0.9, 1.4, 2.7 and 8.3 10^{-3} s^{-1} respectively for 10, 20, 50 and 200 mM at pH 4 and 37°C. These data indicate that for different NaCl concentrations the same stationary state where all enzymes adopt the AR form is reached, but the rate at which it is reached increases upon increasing NaCl concentration.

The influence of chloride on BOD activity as a function of pH was investigated in homogeneous conditions by spectroscopically measuring the BOD activity after 10 min incubation in 100 mM or 200 mM NaCl. As can be seen in Table SI1, the lower the pH the less the activity. No activity can be recovered at pH 4, demonstrating the strong inhibition of BOD at acidic pH in the presence of NaCl. These data suggest the preponderance of the AR form of the BOD at low pH in the presence of NaCl. The influence of pH on chloride inhibition (Fig 5A) was also studied by chronoamperometry at + 0.3 V *vs.* Ag/AgCl.

The electrochemical results confirm the spectrochemical data of Table SI1. Addition of NaCl results in a decrease of the catalytic current which is larger at low pH. After 1200 s, the lower the pH, the lower the current. By combining all the electrochemical data, it is reasonable to assume that in the stationary state, all the enzymes are in the AR form in the presence of NaCl, whose formation is kinetically dependent on pH. From the data in Fig 5A inhibition rates are calculated 2.7, 0.96, 0.38 and 0.22 10^{-3} s^{-1} for pH 4, 5, 6 and 7 respectively at 37°C and 50 mM NaCl. As expected, temperature accelerates the inhibition process (Fig 5B). The inhibition rate constants decrease from 4.9 to 1.6 10^{-3} s^{-1} when temperature is decreased from 50°C to 25°C at pH 4 and 50 mM NaCl.

The value of the reducing potential strongly determines the kinetics of reactivation of the AR form. After addition of NaCl at pH 4, chronoamperometry was performed at various potentials from +0.3 to 0 V. Reactivation of BOD depends on the applied potential, shifting from no reactivation to full reactivation (Fig SI6A). The initial slope of the resulting chronoamperometric signal was measured as a function of the applied reducing potential (Fig SI6B). The more negative the potential, the faster the reactivation. The slopes of reactivation are only slightly affected by the presence (red crosses) or absence of NaCl (blue crosses) in the electrolyte. In the absence of NaCl, they are 12, 5, 0.5 and 0 $\mu A.s^{-1}$ for applied potential of 0, 0.1, 0.2 and 0.3 V vs Ag/AgCl respectively. The limiting current which can be reached also depends on the reducing potential, and the maximum current can only be obtained after removal of NaCl from the electrolyte (Fig SI6C). The currents obtained after NaCl removal (blue crosses) are identical to those obtained before addition of chloride indicating that the observed inhibition is reversible.

One key issue is to determine the conditions in which the AR form can be generated. It is, in particular, important to determine whether O_2 is required or if an oxidative potential alone is sufficient. To address this question, we undertook a series of experiments with *B. pumilus* BOD immobilized on CNFs (Fig 6). In the first experiment, 200 mM NaCl were introduced in a completely deaerated electrolyte while the modified electrode was left at open circuit potential (OCP). The absence of O_2 was confirmed by recording a CV (denoted CV 1 in the chronologic bar) which showed no catalytic current (Fig 6A, blue curve). In a second step, a reducing potential E = 0 V vs Ag/AgCl was applied until all the enzymes were in the reduced state. In a third step, after 10 min at OCP in the presence of 200 mM NaCl in O_2-free buffer, the BOD-modified electrode was directly transferred into a fresh O_2-saturated NaCl-free electrolyte. Finally, a CV was recorded between +0.65V and 0V (Fig 6A, red curve, denoted CV 2). This typical sequence reveals that the enzymes are in the RO form and reduce O_2 at high potential with no requirement of any activation step. Note that under O_2, 10 min at OCP in the presence of NaCl are sufficient to ensure the formation of the AR form (Fig 6B). In a second experiment (Fig 6C), while the first three steps are similar to those described in Fig 6A, an oxidative potential of E = +0.6 V vs Ag/AgCl was applied during 10 min at the modified electrode under anaerobic conditions and in the presence of 200 mM NaCl just after the reductive potential step. The electrode was transferred into a new O_2-saturated electrolyte free of NaCl and a CV was recorded (red curve, Fig 6C). Using this sequence, the voltammogram is characteristic of the reduction of O_2 by the AR form. As can be seen in Fig 6D, a potential of +0.3 V is even sufficient to allow the formation of the AR form. In the absence of Cl^- the resting oxidized form is always obtained (Fig SI7).

These results prove that the formation of the alternative resting form of *B. pumilus* BOD requires the presence of both NaCl and oxidative potential high enough to only oxidize the low potential T3 β Cu while the other TNC Cu's remain reduced. The source of electrons required for this partial reduction might be Cl^-. However, the presence of oxygen is not required (Scheme 1). At pH 7, the RO form has been obtained whatever the experimental conditions (Fig SI8A-F), except for long exposure to 0.3 V potential. This is in agreement with the fact that at neutral pH, 10 min incubation is too short to enable the formation of the AR form, as shown by a chronoamperometry experiments under oxygen (Fig SI8G). Those

data highlight again the importance of the pH on the kinetics of formation of the alternative resting form.

Conclusions

Detailed investigations of the effect of chloride ions on MCOs are of outmost importance for the use of these enzymes for bioelectrochemical applications such as biofuel cells and biosensors, particularly in physiological conditions. This study underlines for the first time the influence of chloride on the direct oxygen reduction by the thermostable bacterial *B. pumilus* BOD, as a function of pH, temperature and potential. The general observation that these parameters have a kinetic effect on chloride inhibition provides insight into the decrease in performances recorded upon long term operation in complex conditions like in physiological media or marine environments[34]. In this study we particularly focus on the occurrence of different resting forms of the enzyme, the fully oxidized RO and the partly oxidized AR forms. The RO/AR interconversion is not specific or unique to BOD from *B. pumilus*. It is a general trait of MCOs containing four coppers. This behavior has been found in MCOs originating both from procaryotes and eucaryotes, and in laccases as well as in BODs. For example, we have recorded the same effect with CotA laccase from *B. subtilis* which shares 67% sequence identity with *B. pumilus*. More interestingly, the same behavior has been observed with BODs from *Myrothecium verrucaria*[9, 10] and *Magnaporthe oryzae*,[10] and with laccase from *Posdopora anserina*,[11] which only share respectively 36%, 23.7% and 22.8% identity with BOD from *B. pumilus*. This clearly indicates that the reported behavior, which was unexplained until our study, is not unique to the BOD from *B. pumilus*. We show here that whether in solution or immobilized at the electrode surface, the RO/AR conversion of a MCO enzyme only occurs in the presence of NaCl, indicating that Cl^- is likely the source of electrons. All our results are also consistent with a model where both the T3β and the T1 are in direct electronic contact with the electroactive surface of the carbon electrode. Once immobilized, the conversion from RO to AR in the presence of NaCl reflects the low redox potential T3β. Considering that 98% of the enzymes used to reduce O_2 are MCOs, the findings reported here are of importance for the catalysis field, and will be especially useful to ensure optimal conditions and applications of BODs in bioelectrochemical devices.

Experimental

Enzymes purification

Bilirubin oxidase (BOD) from *Myrothecium verrucaria* is a gift from Amano (Japan). The production/purification of BOD from *Bacillus pumilus* is described in[26] and the purification of BOD from *Bacillus subtilis* is described in [351].

Modeling

Modelling studies were performed on a 3D model of BOD from *Bacillus pumilus* built by homology to 1GSK (*Bacillus subtilis* BOD) using UCSF chimera molecular modelling package and modeller software.[36, 37] Figures were illustrated using PyMOL (The PyMOL Molecular Graphics System, Version 1.8 Schrödinger, LLC).

UV-visible spectroscopy

UV-visible absorption (UV-vis) spectra were recorded with a Cary-Win UV spectrophotometer equipped with a peltier thermostable multicell holder. All spectroscopic data were obtained with BOD in phosphate-citrate buffer (200-100 mM) at the desired pH. As described in[10] the fully oxidized enzyme was obtained from reduction of as-isolated BOD by dithionite then reoxidation by bubbling O_2 in the solution. Excess dithionite was removed from the reduced enzyme by buffer exchange using a PD 10 column. The effect of sodium chloride on the BOD activity was examined spectrophometrically at 37°C for different NaCl concentrations (0, 100 mM and 200 mM) in citrate-phopshate buffer at pH 4, 5, 6 and 7 by following the oxidation of 1 mM ABTS at 420 nm (ε_{420} nm = 36 mM^{-1} cm^{-1}) and at pH 7 by following the oxidation of 22 µM Syringaldazine (SGZ) at 530 nm (ε_{530} nm = 64 mM^{-1} cm^{-1}). The concentration of BOD was respectively 0.17 nM for the ABTS experiments and 1.7 nM for the SGZ experiments. All experiments were performed in triplicate and standard errors were calculated. The mean of the highest activity was set as 100% of relative activity.

Electrochemical characterization

Electrochemical experiments (cyclic voltammetry, square wave voltammetry and chronoamperometry) were performed with a Bio-Logic potentiostat, using a Ag/AgCl/NaClsat as a reference electrode and a platinum wire as a counter electrode. The working electrode was a pyrolytic graphite (PG, A = 0.07 cm^2) electrode from Bio-Logic modified by carbon nanofibers (CNFs) as described in[38]. BOD was adsorbed on the CNFs as described in[29]. The electrolyte was phosphate-citrate buffer (200-100 mM) at the desired pH. Saturation of the electrolyte was obtained by continuous bubbling of O_2. All potentials are referred to the Ag/AgCl electrode, and the currents are normalized with respect to the maximal current obtained during the experiment. To ensure the total absence of chloride in the experiments without Cl^-, experiments were performed with a silver wire to prevent the presence of Cl^- that may have leaked from the Ag/AgCl reference electrode. Potentials were then calibrated and renormalized. All experiments were performed in triplicate. The mean deviations of calculated inhibition rate constants are 20%.

SWV experiments were performed in 200-100 mM phosphate-citrate buffer at pH 4 and 37°C under N2 atmosphere. The AR form of the enzyme was obtained as described in Fig. 6D, and the enzyme was reactivated as described in Fig. SI4. SWV parameters were: scan rate 5 $mV.s^{-1}$, amplitude 25 mV, frequency 1 Hz.

Supplementary Material

Refer to Web version on PubMed Central for supplementary material.

Acknowledgments

We thank ISM2 laboratory (Marseille) for the kind gift of B. subtilis BOD. We are grateful to Dr M. Ilbert (BIP, Marseille, France) for fruitful discussions, Région Provence-Alpes-Côte d'Azur, Région Aquitaine and ANR for financial support (RATIOCELLS -ANR-12-BS08-0011-01 and CAROUCELL ANR-13-BIOME-0003-02). Part of this work was performed within the framework of the Labex AMADEus (ANR-10-LABX-0042-AMADEus) belonging to the program Initiative d'Excellence IdEx Bordeaux (ANR-10-IDEX-003-02). This work was also

supported by the National Institute of Diabetes and Digestive and Kidney Diseases under NIH grant R01DK31450 (to E.I.S). The content is solely the responsibility of the authors and does not necessarily represent the official views of the National Institutes of Health. C.H.K. acknowledges a John Stauffer Stanford Graduate Fellowship.

Notes and references

1. Mano N, Edembe L. Biosens Bioelectron. 2013; 50:478. [PubMed: 23911663]
2. Solomon EI, Augustine AJ, Yoon J. Dalt Trans. 2008; 3921
3. Solomon EI, Heppner DE, Johnston EM, Ginsbach JW, Cirera J, Qayyum M, Kieber-Emmons MT, Kjaergaard CH, Hadt RG, Tian L. Chem Rev. 2014; 114:3659. [PubMed: 24588098]
4. Heppner DE, Kjaergaard CH, Solomon EI. J Am Chem Soc. 2014; 136:17788. [PubMed: 25490729]
5. Heppner DE, Kjaergaard CH, Solomon EI. J Am Chem Soc. 2013; 135:12212. [PubMed: 23902255]
6. Rulisek L, Ryde U. Coord Chem Rev. 2013; 257:445.
7. Cracknell JA, Blanford CF. Chem l Sci. 2012; 3:1567.
8. Shimizu A, Kwon JH, Sasaki T, Satoh T, Sakurai N, Sakurai T, Yamaguchi S, Samejima T. Biochem. 1999; 38:3034. [PubMed: 10074356]
9. Tasca F, Farias D, Castro C, Acuna-Rougier C, Antiochia R. Plos One. 2015; 10
10. Kjaergaard CH, Durand F, Tasca F, Qayyum MF, Kauffmann B, Gounel S, Suraniti E, Hodgson KO, Hedman B, Mano N, Solomon EI. J Am Chem Soc. 2012; 134:5548. [PubMed: 22413777]
11. Kjaergaard CH, Jones SM, Gounel S, Mano N, Solomon EI. J Am Chem Soc. 2015; 137:8783. [PubMed: 26075678]
12. Xia HQ, Kitazumi Y, Shirai O, Kano K. J Electroanal Chem. 2016; 763:104.
13. Ulyanova Y, Babanova S, Pinchon E, Singhal S, Atanassov P. Phys Chem Chem Phys. 2014; 16:13367. [PubMed: 24875125]
14. Shleev S, Andoralov V, Falk M, Reimannn CT, Ruzgas T, Srnec M, Ryde U, Rulisek L. Electroanalysis. 2012; 24:1524.
15. Lalaoui N, Holzinger M, Le Goff A, Cosnier S. Chem Eur J. 2016; 22:10494. [PubMed: 27328033]
16. Gutierrez-Sanchez C, Ciaccafava A, Blanchard PY, Monsalve K, Giudici-Orticoni MT, Lecomte S, Lojou E. ACS Catal. 2016; 6:5482.
17. Mazurenko I, Monsalve K, Rouhana J, Parent P, Laffon C, Le Goff A, Szunerits S, Boukherroub R, Giudici-Orticoni MT, Mano N, Lojou E. Appl Mater Interfaces. 2016; 8:23074.
18. Ramirez P, Mano N, Andreu R, Ruzgas T, Heller A, Gorton L, Shleev S. Biochim Biophys Acta. 2008; 17771364
19. Ciaccafava A, de Poulpiquet A, Techer V, Giudici-Orticoni MT, Tingry S, Innocent C, Lojou E. Electrochem Comm. 2012; 23:25.
20. Rasmussen M, Abdellaoui S, Minteer SD. Biosens Bioelectron. 2016; 76:91. [PubMed: 26163747]
21. Mano N, Kim HH, Zhang YC, Heller A. J Am Chem Soc. 2002; 124:6480–6486. [PubMed: 12033879]
22. Mano N, Kim HH, Heller A. J Phys Chem, B. 2002; 106:8842–8848.
23. Kim HH, Zhang YC, Heller A. Anal Chem. 2004; 76:2411–2414. [PubMed: 15080757]
24. Hirose J, Inoue K, Sakuragi H, Kikkawa M, Minakami M, Morikawa T, Iwamoto H, Hiromi K. Inorg Chim Acta. 1998; 273:204.
25. Dagys M, Laurynenas A, Ratautas D, Kulys J, Vidziunaite R, Talaikis M, Niaura G, Marcinkeviciene L, Meskys R, Shleev S. Energy Environ Sci. 2016
26. Durand F, Kjaergaard CH, Suraniti E, Gounel S, Hadt RG, Solomon EI, Mano N. Biosen Bioelectron. 2012; 35:140.
27. Edembe L, Gounel S, Cadet M, Durand F, Mano N. Electrochem Comm. 2012; 23:80.
28. Suraniti E, Tsujimura S, Durand F, Mano N. Electrochem Comm. 2013; 26:41.
29. de Poulpiquet A, Ciaccafava A, Gadiou R, Gounel S, Giudici-Orticoni MT, Mano N, Lojou E. Electrochem Comm. 2014; 42:72.
30. Cracknell JA, Vincent KA, Armstrong FA. Chem Rev. 2008; 108:2439–2461. [PubMed: 18620369]

31. dos Santos L, Climent V, Blanford CF, Armstrong FA. Phys Chem Chem Phys. 2010; 12:13962–13974. [PubMed: 20852807]
32. Christenson A, Shleev S, Mano N, Heller A, Gorton L. Biochim Biophys Acta-Bioenerg. 2006; 1757:1634–1641.
33. Page CC, Moser CC, Chen X, Dutton PL. Nature. 1999; 402:47. [PubMed: 10573417]
34. Santoro C, Babanova S, Erable B, Schler A, Atanassov P. Bioelectrochemistry. 2016; 108:1–7. [PubMed: 26544631]
35. Bento I, Martins LO, Lopes GG, Carrondo MA, Lindley PF. Dalton Transactions. 2005; 21:3507.
36. Pettersen EF, Goddard TD, Huang CC, Couch GS, Greenblatt DM, Meng EC, Ferrin TE. J Comput Chem. 2004; 25:1605. [PubMed: 15264254]
37. Fiser A, Šali A. Methods in enzymology. 2003; 374:461. [PubMed: 14696385]
38. de Poulpiquet A, Marques-Knopf H, Wernert V, Giudici-Orticoni MT, Gadiou R, Lojou E. Phys Chem Chem Phys. 2014; 16(4):1366. [PubMed: 24296569]

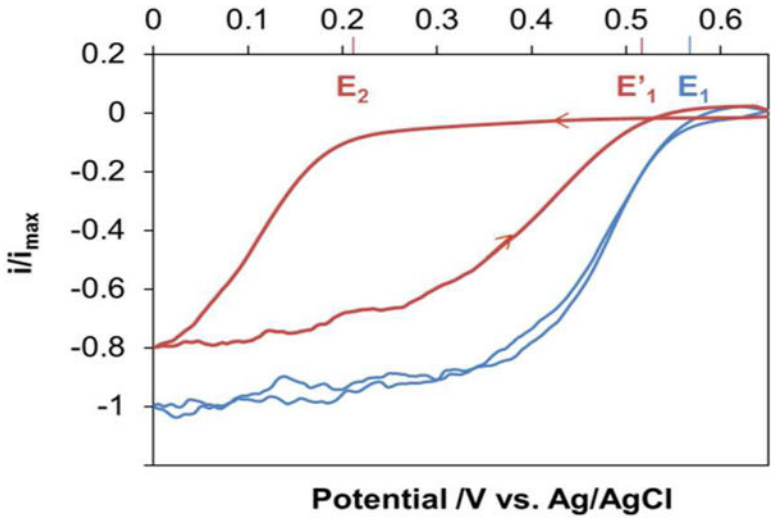

Figure 1.

Influence of NaCl at pH 4 and 37°C: cyclic voltammogram of O_2 reduction by *B. pumilus* BOD at 5 $mV.s^{-1}$ in 200-100 mM phosphate-citrate buffer. Blue curve: usual catalytic response in the absence of NaCl. Red curve: hysteresis observed after 15 mM NaCl addition. The arrows indicate the direction of the potential sweep. The pyrolytic graphite electrode was first modified with carbon nanofibers and then with BOD.

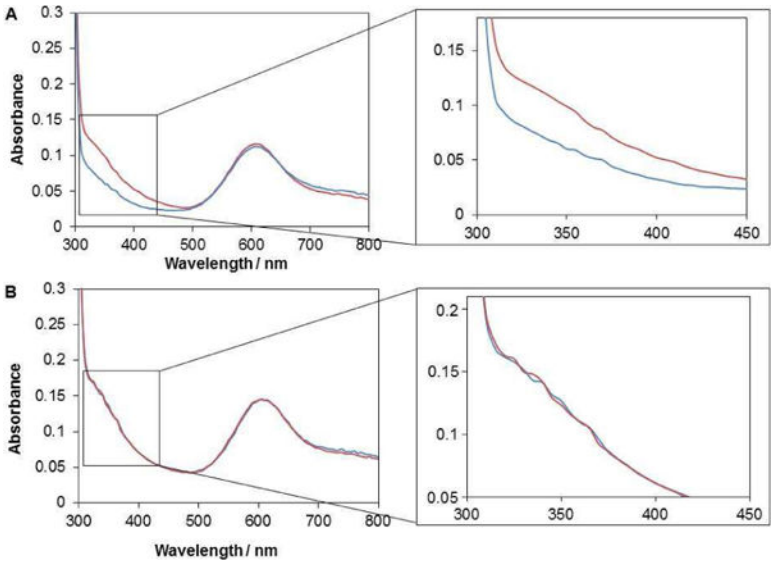

Figure 2.

UV-visible spectra of *B. pumilus* BOD at 25°C and at (A) pH 4, and (B) pH 7; As isolated enzyme before (red curve), and after 200 mM NaCl addition (blue curve). The graph on the right is a zoom on the 330 nm shoulder.

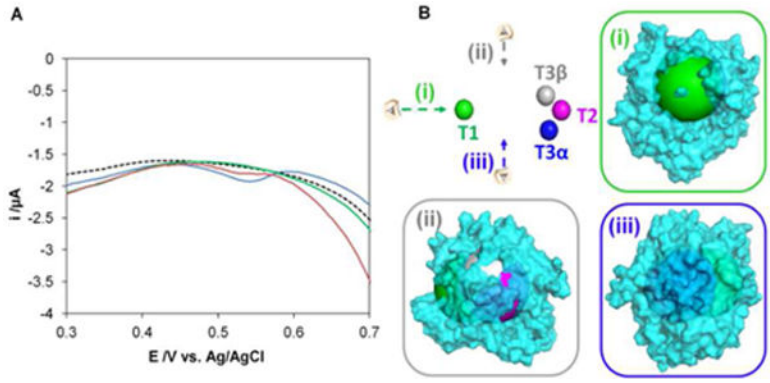

Figure 3.

Electrical connection of the Cu centers in *B. Pumilus* BOD. (A) Square Wave Voltametry (SWV) of the immobilized *B. pumilus* BOD at pH 4 and 37°C in 200-100 mM phosphate-citrate buffer under anaerobic conditions. RO form of the enzyme (blue line), AR form of the enzyme after NaCl addition (green line), and reactivated enzyme obtained as described in Fig. SI4 (red line). The attribution of the peak to the T1 Cu is confirmed by the corresponding potential and a comparison with the signal of the bare electrode (black dashed line). SWV parameters: 5 $mV.s^{-1}$, amplitude 25 mV, frequency 1 Hz. Electrode modified as in Fig 1. (B). Illustration of electron accessibility from protein surface to copper centers in the BOD from *B. Pumilus*. Top left: Copper centers only from the 3D model of BOD are represented by spheres, and colored, T1 (green) T3β (grey) T3α (blue) and T2 (Pink). Views (i), (ii) and (iii): Three representations of semi-transparent molecular surface of the BOD colored in cyan and showing spheres with 15 Å of radius centered on each copper atom. Spheres are colored with respect to the corresponding copper site. The distance from the surface of the protein to each copper center is less than 15 Å except for the T3α. Protein representations were generated using the program PyMOL (The PyMOL Molecular Graphics System, Schrödinger, LLC).

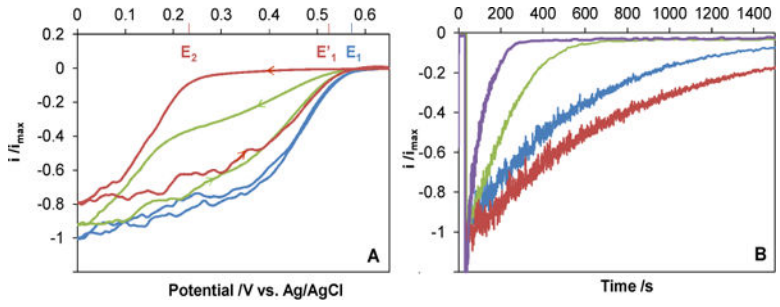

Figure 4.

O_2 reduction by *B. pumilus* BOD at pH 4 and 37°C. (A) CV curves at 5 $mV.s^{-1}$ in 200-100 mM phosphate-citrate buffer. 15 min incubation in increasing NaCl concentrations: 0 mM (blue curve), 5 mM (green curve) and 20 mM (red curve, note that higher NaCl concentrations result in the same CV shape) (B) Chronoamperometric measurement at E = + 0.3 V vs Ag/AgCl with increasing NaCl concentrations: 10 mM (red curve), 20 mM (blue curve), 50 mM (green curve) and 200 mM (purple curve). Electrodes modified as in Fig 1.

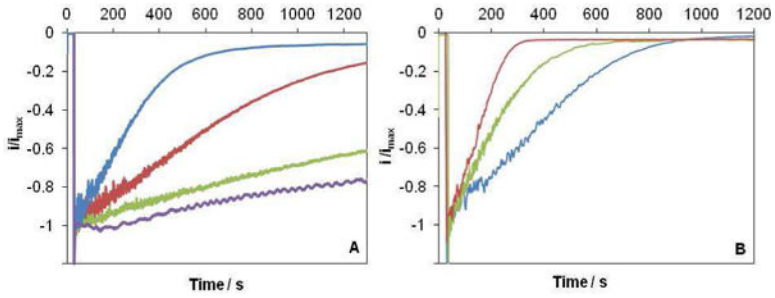

Figure 5.

Kinetics of O_2 reduction inhibition by NaCl. Chronoamperometric measurement at E = +0.3 V *vs.* Ag/AgCl (A) as a function of pH at T = 37°C and 50 mM NaCl: pH 4 (blue curve), pH 5 (red curve), pH 6 (green curve) and pH 7 (purple curve); (B) as a function of temperature at pH 4 and 50 mM NaCl: T = 25°C (blue curve), T = 37°C (green curve), T = 50°C (red curve). O_2-saturated 200-100 mM phosphate-citrate buffer. Electrodes modified as in Fig 1.

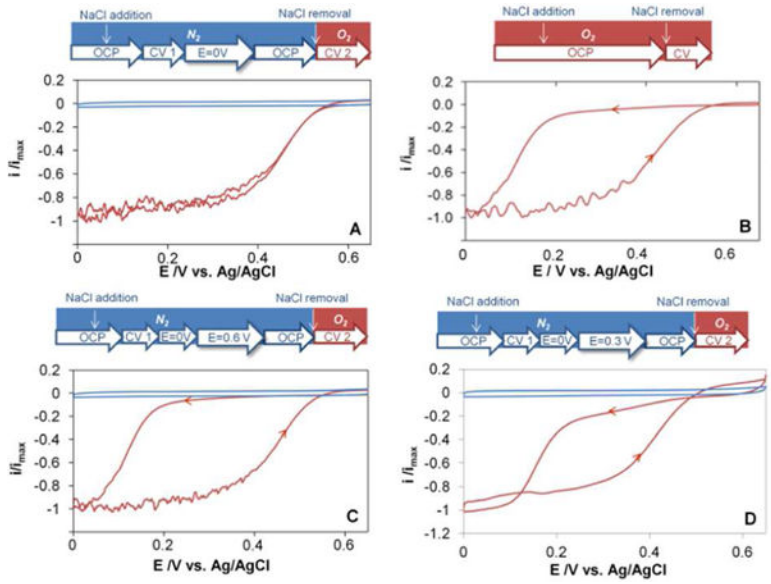

Figure 6.

Oxidative requirements for the formation of the resting oxidized form (A) or the alternative resting form (B, C and D) of *B. pumilus* BOD. (A) CV curves under N2 (blue curve) and under O_2 (red curve) after the CV sequence described in the chronologic bar; (B) CV curve under O_2 after the enzyme has been exposed to 200 mM NaCl under O_2; (C) CV curves under N2 (blue curve) and under O_2 (red curve) after the CV sequence described in the chronologic bar. (D) CV curves under N2 (blue curve) and under O_2 (red curve) after the CV sequence described in the chronologic bar. 5 $mV.s^{-1}$ in phosphate-citrate buffer, 200-100 mM pH 4, T = 37 °C.

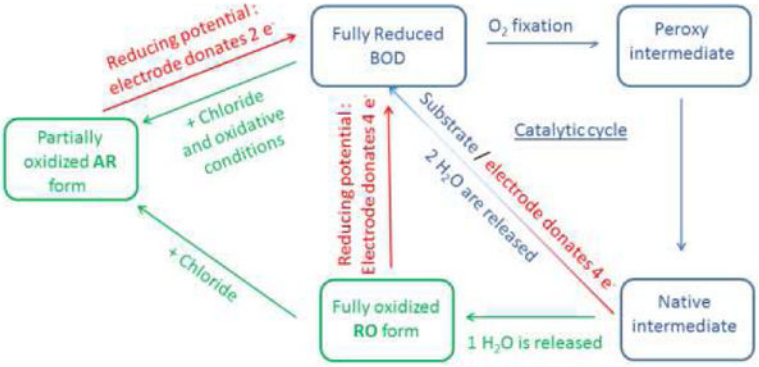

Scheme 1.

A mechanism of the O_2 reduction by BODs based on Solomon *et al.*[2,11] with our additions concerning the AR formation and reactivation in the presence of chloride ions. The catalytic cycle is drawn in blue, the non-catalytically relevant forms are drawn in green, and electrode induced redox changes are indicated in red.